Relaxation Processes in Room Temperature Ionic Liquids: The Case of 1-Butyl-3-Methyl Imidazolium Hexafluorophosphate

Alessandro Triolo,*,† Olga Russina,‡ Christopher Hardacre,§ Mark Nieuwenhuyzen,§ Miguel Angel Gonzalez,|| and Hans Grimm⊥

Istituto per i Processi Chimico-Fisici, Consiglio Nazionale delle Ricerche, via La Farina 237, 98123 Messina, Italy, Hahn-Meitner Institut, Glienicker Str. 100, D-14109 Berlin, Germany, QUILL Research Centre and School of Chemistry, Queen's University, Belfast BT9 5AG, Northern Ireland, Institut Laue Langevin, 6, rue J. Horowitz, BP 156, 38042 Grenoble Cedex 9, France, and Institut für Festkörperforschung, Forschungs Zentrum Jülich GmbH, D-52425 Jülich, Germany

Received: June 21, 2005; In Final Form: September 21, 2005

A detailed investigation on the nature of the relaxation processes occurring in a typical room temperature ionic liquid (RTIL), namely, 1-butyl-3-methyl imidazolium hexafluorophosphate ([bmim][PF_6]), is reported. The study was conducted using both elastic and inelastic neutron scattering over a wide temperature range from 10 to 400 K, accessing the dynamic features of both the liquid and glassy amorphous states. In this study, the inelastic fixed energy scan technique has been applied for the first time to this class of materials. Using this technique, the existence of two relaxation processes below the glass transition and a further diffusive process occurring above the glass−liquid transition are observed. The low temperature processes are associated with methyl group rotation and butyl chain relaxation in the glassy state and have been modeled in terms of two Debye-like, Arrhenius activated processes. The high temperature process has been modeled in terms of a Kohlraush−Williams−Watts relaxation, with a distinct Vogel−Fulcher−Tamman temperature dependence. These results provide novel information that will be useful in rationalizing the observed structural and dynamical behavior of RTILs in the amorphous state.

Introduction

Room temperature ionic liquids are increasingly attracting attention as nonmolecular liquid media for a wide range of applications[1] including as solvents for reactive chemistry, as electrolytes, as liquid crystalline materials, and as extractants. This is due to their inherent conducting properties, the ability to tune the physical properties of the liquid by changing the anion−cation combination, and the effect of ionic interactions on solvation, for example, compared with molecular interactions found in water, supercritical fluids, and organic solvents. As part of an ongoing investigation into the structure of ionic liquids and the dynamics within the liquids, this study describes quasi-elastic neutron scattering (QENS) on 1-butyl-3-methyl imidazolium hexafluorophosphate ([bmim][PF_6]), shown in Figure 1.

A number of studies have examined the structure of ionic liquids using simulations,[2−4] X-ray scattering,[5−7] and neutron[8,9] scattering; however, the dynamics in ionic liquids has been studied in much less detail. Recently, Triolo et al.[10] examined the dynamics of [bmim][PF_6] using QENS between 250 and 320 K. Two different dynamic processes were found to exist in the sub-picosecond and sub-nanosecond temporal window, with each having a different temperature and momentum transfer dependence. These findings are in reasonable agreement with results from molecular dynamics simulations.[4] In addition, the reorientational dynamics of [bmim][PF_6] have been investigated using ^{13}C NMR techniques.[11] From modeling of the spin−lattice relaxation constants and nuclear Overhauser effects, two motions have also been elucidated, a fast molecular motion and a slower rotational diffusion process. Giraud et al. also examined the reorientional dynamics using the Kerr effect.[12] Urahata and Ribeiro have recently reported an extensive molecular dynamics study examining the dynamics as a function of alkyl chain length in 1,3-dialkylimidazolium ionic liquids and anion size.[13] The mean square displacement was found to have a maximum with alkyl chain length at C_4. In addition, the displacement of the cations was found to be larger with increasing anion size. As found from the NMR studies, the molecular dynamics showed a strong anisotropic dynamic motion due to the rapid motion of the alkyl chain and the much slower rotation of the whole cation.

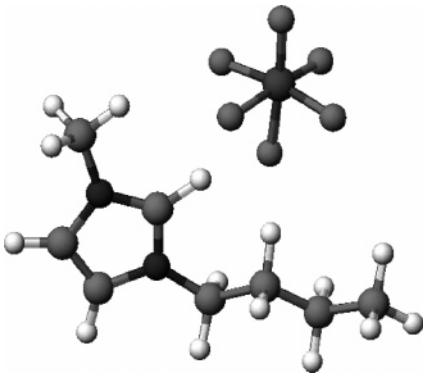

Figure 1. Schematic representation of 1-butyl-3-methyl imidazolium hexafluorophosphate ([bmim][PF_6]).

* Corresponding author. E-mail: triolo@me.cnr.it.
† Consiglio Nazionale delle Ricerche.
‡ Hahn-Meitner Institut.
§ Queen's University.
|| Institut Laue Langevin.
⊥ Institut für Festkörperforschung.

10.1021/jp053355j CCC: $30.25
Published on Web 10/25/2005

By using selectively deuterated and protiated samples of [bmim][PF_6], this study uses QENS to discriminate between the processes due to the dynamics of the methyl and butyl groups as well as those associated with the diffusion of the whole molecule.

Experimental Section

Protiated 1-butyl-3-methyl imidazolium hexafluorophosphate ([bmim][PF_6]) was obtained from Merck. The selectively deuterated hexafluorophosphate samples were prepared from butyl-deuterated and methyl-deuterated 1-butyl-3-methyl imidazolium chloride salts[14] by metathesis with NH_4PF_6 to form the d_9-[bmim][PF_6] and d_3-[bmim][PF_6] salts, respectively. In each case, the standard procedure was followed.[15] Each sample was analyzed by ^1H and ^2H NMR as well as by elemental analysis and showed >97% deuterium incorporation. All samples were dried as liquids under high vacuum at 333 K, cooled, and transferred to the sample containers under N_2 prior to performing the QENS measurements,

QENS measurements were collected at three backscattering spectrometers.

Elastic fixed energy scans (EFESs) were collected at both IN16 and IN10 at the Institute Laue Langevin (ILL) using $\lambda = 6.271$ Å, accessing a Q range between 0.43 and 1.90 Å^{-1}, with an energy resolution of 0.9 μeV. The EFES data were collected as a function of temperature by monitoring the number of neutrons that were elastically scattered by the sample, upon heating or cooling the sample, following removal of the constant contribution from the empty cell and normalization to the detector efficiency using vanadium. The measurements were collected from samples contained in cylindrical annular aluminum cells with a sample thickness between 0.1 and 0.5 mm in order to minimize multiple scattering effects. To access the dynamical features related to the amorphous glass, cooling from the melt was chosen in order to avoid crystallization of the sample which occurs upon heating the glassy amorphous phase. The samples were investigated between ~10 to 450 K using heating/cooling rates of 1.3 K min^{-1}. Using the same conditions, EFESs were also collected at IN10, which is a backscattering spectrometer similar to IN16.

Inelastic fixed energy scans (IFESs)[16] were collected at the BSS spectrometer at the Forschungs Zentrum Jülich (FZJ) using an energy resolution of approximately 1 μeV, covering a Q range between 1.02 and 1.87 Å^{-1}. During the measurements, the number of neutrons that were scattered from the sample with an energy exchange of 14.15 μeV was monitored upon heating/cooling, covering a temperature range between 10 and 450 K. The same cylindrical annular sample geometry used at the ILL was used for these experiments.

Results

The EFESs were examined in order to extract qualitative information on the possibility of separating different dynamical processes in [bmim][PF_6]. Three data sets collected on IN16 are shown in Figure 2 following a cyclic thermal path, namely, cooling from the liquid to the glass at ~10 K at 1.3 K min^{-1}, heating the glass to the liquid state, and a second cooling from the liquid to the glass. It is clear that when cooling the liquid no crystallization is observed even after extended periods of time. However, as expected, upon heating, the glass crystallized above the glass transition temperature ($T_g = 190$ K) between 210 and 220 K. The signature of this process is the discontinuous increase of the EFES signal, indicating the formation of a phase which is rigid on the time scale associated with the accessible

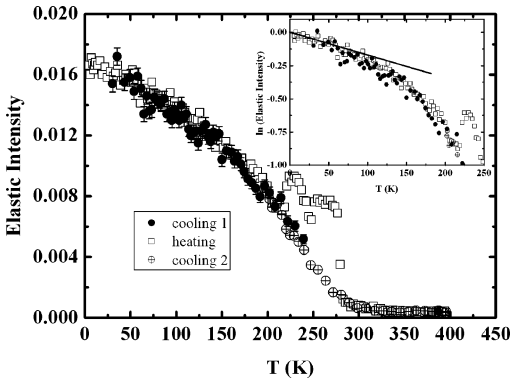

Figure 2. Elastic fixed energy scans collected on 1-butyl-3-methyl imidazolium hexafluorophosphate ([bmim][PF_6]) at IN16, at fixed $Q = 1.89$ Å^{-1}. For the data referring to the first cooling stage, experimental error bars are reported. In the inset, the natural logarithm of the EFE intensity is plotted versus temperature, to highlight the initial linear behavior for $T > 60$ K. Above that temperature, relaxation processes become active at the time scale probed by the spectrometer.

instrumental energy resolution. In addition, upon crystallization, clear Bragg peaks were also observed, despite the low Q resolution available at IN16. Above the melting point of the crystalline phase ($T_m = 284$ K), the EFE intensity decreased to a value which is consistent with the formation of a liquid. The second cooling curve is superimposable on the initial cooling data, showing a high degree of reproducibility and a qualitative estimation of experimental error bars.

Further inspection of the inset of Figure 2 shows the existence of a low temperature range ($T < 60$ K) where ln(elastic intensity) $\propto -T$. This behavior is consistent with a Debye−Waller effect due to the rapid oscillations of hydrogen atoms around their equilibrium positions. Above ~60 K, the experimental data deviate from this linear behavior (see the inset of Figure 2). Such a behavior is related to the triggering of energy exchange between neutrons and relaxation processes which become thermally activated. The further decrease in EFE intensity above 200 K is due to the glass-to-liquid transition when the diffusive processes get activated.

The inspection of Figure 2 suggests that the EFES data from a fully protiated sample can only provide qualitative information. To extract more specific information, partially deuterated [bmim][PF_6] samples were also examined. The large difference between the scattering cross sections of H (which is a fundamentally incoherent scatterer) and D (which has a total cross section that is 11 times smaller than that of H and is a mainly coherent scatterer) causes the partial suppression of the incoherent scattering contribution of the deuterium-labeled portions, though it also leads to a concomitant increase in the coherent scattering. It should be noted that a quantitative fitting of the data was not possible from partially deuterated samples because of the superposition of the coherent and incoherent scattering from hydrogen, deuterium, carbon, and nitrogen. The inset of Figure 3 shows EFES data collected on IN10 for the butyl- and methyl-deuterated samples at $Q = 1.85$ Å^{-1}. The selective deuteration accentuates the incoherent signal from the remaining hydrogenated sites, although the effect of additional coherent contributions to the scattering is not negligible, especially for the d_9-[bmim][PF_6] sample. As expected, the EFE data from the d_3-[bmim][PF_6] and protiated [bmim][PF_6] (Figure 2) samples are quite similar due to the fact that only the three methyl group hydrogen atoms have been replaced. In comparison, a reproducible sharp decrease in the EFE intensity appears in the low temperature region (10−80 K) from the d_9-[bmim][PF_6] sample. This feature is the consequence of the activation

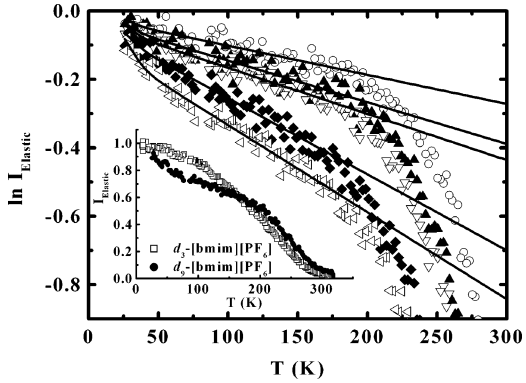

Figure 3. Elastic fixed energy scans collected at IN10 on selectively deuterated d_9-[bmim][PF_6], at different Q values (Q = 1.18, 1.45, 1.68, 1.85, and 1.96 Å^{-1}, respectively, from top to bottom). The lines correspond to the fit described in the text, accounting for the relaxation of the methyl group. In the inset, data from the two selectively deuterated samples—d_9-[bmim][PF_6] and d_3-[bmim][PF_6]—are compared at a selected Q value (Q = 1.85 Å^{-1}).

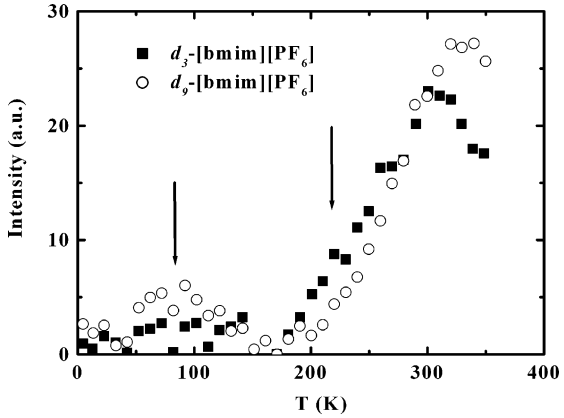

Figure 4. Comparison between inelastic fixed energy scans collected at BSS from the two selectively deuterated samples, d_9-[bmim][PF_6] and d_3-[bmim][PF_6], at a selected Q value (Q = 1.52 Å^{-1}).

of the methyl group rotation. This relaxation feature is not directly visible in Figure 2 because it is masked by the incoherent scattering from the butyl chain that dominates the spectra. Although similar EFES data have also been observed from materials containing methyl groups, such as polymers (e.g., polyisoprene, polypropylene), and show an equivalent decrease in intensity, this feature is generally observed at much higher temperatures (100−120 K), that is, when the rotation motion of the $-CH_3$ units becomes thermally activated. The fact that this feature is observed in d_9-[bmim][PF_6] at a lower temperature indicates a much lower activation energy for the corresponding motion in the ionic liquid.

The EFES data from d_9-[bmim][PF_6] were modeled according to an Arrhenius-like activated process, with a jumping rate, $\Gamma(T)$, given by

$$\Gamma(T) = \Gamma_0 \exp[-E_{act}/k_B T] \quad (1)$$

where Γ_0 is the attempt frequency at high temperature and E_{act} is the activation energy. The fit of the experimental data in terms of this model is shown in Figure 3. Attempts to account for a distribution of activation energies, as is commonly found necessary in polymeric glassy materials, did not lead to a substantial improvement in the modeling. In addition, the width of the log-Gaussian distribution (eq 2) used to describe the rotational rate distribution[17] was negligible, thus indicating that the distribution is essentially monodisperse:

$$g(E) = 1/(\sigma(2\pi)^{0.5}) \exp(-(E - \langle E_{act}\rangle)^2/(2\sigma^2)) \quad (2)$$

Using a well-established procedure[18] and assuming a Lorentzian shape for the quasi-elastic broadening, the EFES was modeled according to

$$S(Q;\omega\sim 0) = A_0(Q) + 2/\pi[1 - A_0(Q)] \operatorname{arctg}(\Gamma_r/\Gamma) \quad (3)$$

where Γ_r is the width of the instrumental resolution (0.9 μeV) (eq 3 assumes a rectangular shape for the instrumental resolution), $A_0(Q)$ is an apparent elastic incoherent structure factor due to the combination of coherent and incoherent scattering and is a fitted parameter of the model, and (Γ_r/Γ) is given by eq 1.

$$S(Q;\omega\sim 0) = \mathrm{DWF}(A_0(Q) + 2/\pi[1 - A_0(Q)] \operatorname{arctg}(\Gamma_r/(\Gamma_0 \exp[-E_{act}/k_B T]))) \quad (4)$$

Within eq 4, DWF represents the Debye−Waller factor contribution:

$$\mathrm{DWF} = \exp[-0.333 Q^2 \langle r^2\rangle]$$

where $\langle r^2\rangle$ is the mean square displacement, which was assumed to be linearly dependent with temperature, that is, $\langle r^2\rangle = \langle r_0^2\rangle + \mathrm{d}\langle r^2\rangle/\mathrm{d}T * T$.

In Figure 4, a comparison between IFE scans from both d_3- and d_9-[bmim][PF_6] is reported. One can observe that the main features of these data reflect the activation of the relaxation processes of the butyl and methyl side group, respectively. In particular, excess intensity, indicated by the arrows, is found centered at 80 K for d_9-[bmim][PF_6] and at ∼220 K for d_3-[bmim][PF_6]. These features are the signatures of the two group relaxation processes. Upon selective deuteration, it is possible to separate the butyl or methyl group contributions and hence observe relaxation of the remaining protiated units, that is, the methyl group at 80 K and the butyl chain at 220 K.

The low temperature (T < 180 K) portion of the EFES from sample d_9-[bmim][PF_6] was modeled (fit reported in Figure 3) in terms of the above-described formalism together with the IFES data on the same sample. Using this fitting procedure, values of Γ_0 = 0.17 meV, E_{act} = 1.28 kJ mol^{-1}, and $\mathrm{d}\langle r^2\rangle/\mathrm{d}T$ = 0.0025 Å^2 K^{-1} were derived.

Due to the combination of coherent and incoherent scattering arising from the chemical (and isotopic) composition of the sample, it was not feasible to extract geometrical information on the nature of this process from the Q dependence of the signal. This is only achievable by examining the elastic incoherent structure factor (EISF) which can be extracted as the ratio between the elastic scattering and the total (elastic + inelastic) scattering, as a function of Q. However, as the IFES does not monitor the elastic signal, but only the inelastic one, the EISF cannot be calculated from these data. Despite the absence of low temperature features in the protiated [bmim]-[PF_6] EFES data (Figure 2), the IFES data from this sample, shown in Figure 5a, clearly show the existence of the CH_3 rotation process, as indicated by the low amplitude peak centered at ∼80 K. This correlates well with the temperature where the methyl group relaxation was observed in d_9-[bmim][PF_6] (Figure 4).

Further analysis of the IFES data from protiated [bmim][PF_6] (Figure 5a) shows that, in addition to the first relaxation process, it is possible to characterize two further dynamical processes occurring above 150 K. An inspection of the molecular structure of [bmim][PF_6], together with the evidence from Figure 4,

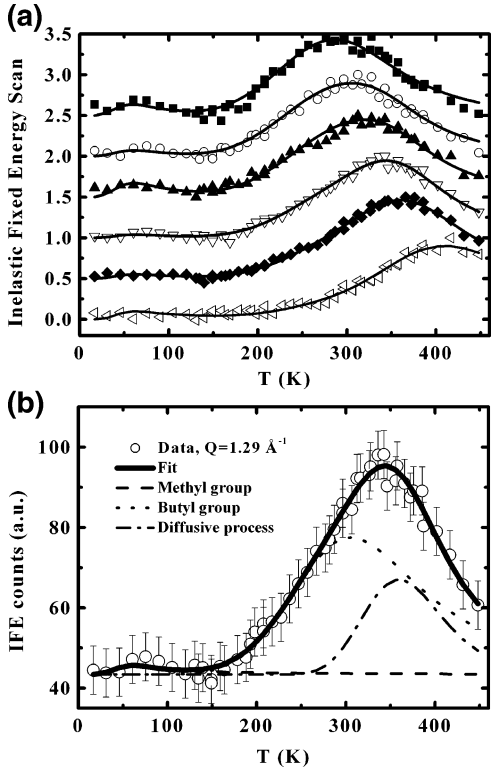

Figure 5. (a) Inelastic fixed energy scans collected on [bmim][PF_6], at different Q values (Q = 0.56, 1.02, 1.29, 1.52, 1.72, and 1.87 Å^{-1}, respectively, from top to bottom). The lines correspond to the fits in terms of the model described in the text, accounting for the two localized processes and the diffusive one. (b) Detailed description of the modeling of the inelastic fixed energy scan collected at BSS from [bmim][PF_6], at a selected Q value (Q = 1.29 Å^{-1}). The contributions associated with the methyl and butyl group relaxations and to the diffusive dynamics are plotted.

suggests that the process found between 200 and 300 K is likely to be associated with the relaxation of the butyl chain. At higher temperatures, this is followed by the diffusive dynamics associated with the glass-to-liquid transition. As these processes overlap in the accessible Q range, their modeling is a complex task. However, as a Q dependence is found for the diffusive dynamics but no Q dependence of the butyl dynamics is expected, since this motion can be considered to be a localized, nondiffusive one, at suitably chosen Q values, the two processes will be well separated. To enable a full separation, Q values lower than ~1.0 Å^{-1} would be needed; however, this was not possible using the present experimental setup, and therefore, at the Q values shown in Figure 5a, the two processes are still partially superimposed. Still, taking advantage of the different Q dependences for the two processes, it is possible to extract useful information on their nature.

As described for the methyl rotation process, the butyl chain motion is assumed to relax via an Arrhenius-like activated route. Again, the modeling did not require the assumption of a heterogeneous environment experienced by the butyl moiety and a single activation energy could be used to satisfactorily describe the data.

The diffusive dynamics process is known to show non-Arrhenius features and may be fitted using the Vogel−Tammann−Fulcher (VTF) expression:[19−21]

$$\tau(Q,T) = \tau_0(Q)\exp[E_{act,app}/k_B(T - T_0)] \quad (5)$$

where $\tau(Q,T)$ is the characteristic time for the relaxation at temperature T and momentum value Q and $\tau_0(Q)$ is the inverse of the attempt frequency for the process at infinite temperature. $E_{act,app}$ is the apparent activation energy for the process, and T_0 is a characteristic temperature accounting for the deviation from the Arrhenius law. τ_0 is dependent on Q via $\tau_0(Q) \sim Q^{-\nu}$, where ν is a characteristic exponent. In addition, the temporal shape of this relaxation is typically different from that described by the Debye law; in general, this process is described in terms of the Kohlrausch−Williams−Watt (KWW) expression[22] (eq 6):

$$\phi(t) = \exp(-t/\tau)^{\beta} \quad (6)$$

where τ is a characteristic time for the relaxation and β ($0 < \beta \leq 1$) is a parameter accounting for deviations from the exponential (Debye) law. The KWW expression is defined in the temporal domain, and an analytical expression for its frequency dependence only exists for selected values of β. Recently, an efficient numerical procedure for Fourier transformation of the KWW expression into the frequency domain has been developed.[23] This routine has been used to evaluate the temperature dependence of the IFES at fixed frequency (ω_{ifw} = 14.15 μeV). Using this procedure, optimized values for the fitting parameters $d\langle r^2\rangle/dT$, $\Gamma_{0,butyl}$, $E_{act,butyl}$ (referring to the butyl relaxation), $\tau_{0,\alpha}(Q)$, β, ν, $E_{act,app}$, and T_0 (referring to the diffusive or α-process) were obtained. An adjustment of the IFES background, BKG, and the amplitudes, A_i, of the butyl relaxation and diffusive dynamics processes was also required. The overall model used is described in eq 7 including the numerical procedure to evaluate the Fourier Transform (FT):

$$\mathrm{IFES}(T>200\mathrm{K}) = \mathrm{BKG} + \mathrm{DWF}(A_{butyl}2/\pi\Gamma(E_{act,butyl})/[\omega_{ifw}{}^2 + \Gamma(E_{act,butyl})^2] + A_\alpha \mathrm{FT}[\exp(-t/\tau)^{\beta}]) \quad (7)$$

Figure 5a shows the offset normalized experimental data together with the fitting curves from eq 7. Figure 5b shows the single components to these fits for a selected value of Q. The parameters from the modeling of the two processes (butyl relaxation and diffusive dynamics) are shown in Table 1.

TABLE 1: Fitting Parameters Obtained by the Modeling of the IFES Data from [bmim][PF_6] in Terms of Equation 7

parameter	value
$\Gamma_{0,butyl}$	0.91 meV
$E_{act,butyl}$	11.34 kJ mol^{-1}
β	0.42
ν	2.7
$E_{act,app}$	17.1 kJ mol^{-1}
T_0	170 K

The DWF term $d\langle r^2\rangle/dT$ was determined from the simultaneous fitting of the curves over the whole accessible temperature range leading to $d\langle r^2\rangle/dT = 0.0025$ Å^2 K^{-1}. The amplitudes of the two high temperature processes shown in Figure 5b show a distinct Q dependence. In particular, with increasing Q, the amplitude of the diffusive dynamics process decreases. This might be a consequence of the geometrical features of the butyl chain motion.

Discussion

It is clear that the IFES experimental approach provides very useful information that is complementary to that which is accessible through the more traditional EFES approach. Despite this advantage, there are very few examples of IFES studies of soft matter and those which have been reported have been limited to polymeric materials.[16,24] This approach allows the existence of relaxation processes occurring in the spatial-temporal window accessible to the spectrometer to be identified easily and without bias.

The previous QENS characterization of the dynamics in [bmim][PF_6][10] indicated two relaxation processes, a fast localized process and a slower diffusive motion. Although this model is qualitatively confirmed by the present study, the detailed quantitative analysis has led to different conclusions. The preliminary data set collected at the FOCUS time-of-flight spectrometer covered the temperature range between 250 and 320 K and the Q range between 1.4 and 2.2 $Å^{-1}$.[10] On the basis of the IFES data and modeling reported herein (Figure 5a,b), the former QENS data were mainly probing the butyl relaxation. Such a finding is very instructive on the limitations/requirements of the experimental approach that we are presently employing. The possibility of accessing a temperature scan at a fixed energy exchange provides a clear indication of the number and nature of dynamic processes occurring in the sample as a function of Q and T. Although more complete, a series of isothermal QENS patterns (over a range of frequencies) often do not provide the same qualitative, fundamental information.

A number of investigations into the dynamics of ionic liquids have shown the presence of two relaxation time scales. This study clearly highlights the presence of a third methyl rotation process which has not been reported previously in ionic liquids due to the time constant being outside that probed by the NMR, for example.[11] The motions above and below T_g are similar to those found in neat polypropylene oxide, for example, where the methyl rotation occurs in the glass state and skeletal motions occur in the liquid.[16] It is interesting to note that, despite the similarities, the activation barrier for the methyl relaxation process is much lower than that in polymers. Such an activation barrier ranges from 3.7 to >5 kJ mol^{-1} for some polymers.[25]

Our description of the experimental data leads to a surprisingly low value for the activation energy for the methyl group rotation. Even in the case of gas phase, low molecular weight molecules, the barrier for the methyl group rotation ranges from 2 to 11 kJ/mol.[26] We can be conclusive in stating that our QENS data indicate a low activation energy for the rotation of the methyl group (as indicated by the occurrence of relaxation features at a much lower temperature than that observed, e.g., in poly(propylene oxide) (see ref 16)). However, due to the low signal-to-noise ratio and to the possible coupling between fitting parameters, we realize that further measurements are required to obtain a conclusive estimation of the activation parameters for the methyl group rotation.

The anomalously low activation barrier is possibly due to the weak hydrogen bonding of the $[PF_6]^-$ anion. In the liquid structure of 1,3-dimethyl imidazolium hexafluorophosphate ([dmim][PF_6]), the anion interacts with the imidazolium ring hydrogens but only limited anion density is found around the methyl groups, indicating only a weak interaction, as expected.[9] In addition, in the crystal and liquid structures of [dmim][PF_6], only short methyl hydrogen−methyl hydrogen contacts are found, whereas the chloride structures also show methyl hydrogen−ring hydrogen contacts. Therefore, it should be expected that both the constraints due to cation−cation and cation−anion interactions for the methyl group rotation will be much weaker than those for other systems, such as the chloride salts. This is in agreement with simulations of the crystal structures of [dmim]Cl and [dmim][PF_6].[3] Using a united atom approach for the methyl groups, where the CH_3 is replaced by a sphere of the correct size and a given charge, gave reasonable agreement with the experimentally determined structure, as well as similar data to those obtained from the explicit methyl group, in the case of the $[PF_6]^-$ anion, whereas substantial differences were observed for the chloride salt. These simulations indicate the importance of methyl hydrogen interactions with the anion and cation in the case of chloride and the absence of strong specific interactions for the hexafluorophosphate resulting in the low activation barrier observed. The fact that there is also no need to introduce an appreciable degree of polydispersity in the activation energy for this process also indicates either that all of the methyl groups are in similar environments, which is likely, or that despite the variation in environment the methyl groups are not constrained. This may be compared with the situation in amorphous polymer glasses, where the methyl group motion is described in terms of a distribution of rotational rates and activation energies.[17]

There is limited information available on the features of the liquid−glass transition in room temperature ionic liquids (RTILs), in general, and in [bmim][PF_6] in particular. There is even less information available on the nature of sub-T_g processes in this class of materials. Self-diffusion coefficients in [bmim][PF_6] have been derived in the liquid state from NMR measurements, indicating a non-Arrhenius temperature dependence for this process.[27]

Many molecular dynamics simulation studies[2−4] have been developed to describe both structural and dynamical features of RTILs, although no efforts have been paid so far to the characterization of local processes or to the temperature dependence of the diffusive dynamics.

To the best of our knowledge, no other studies exist which can be compared directly with the present results on the local dynamics of the methyl and butyl groups. A QENS investigation[28] of the dynamics in liquid butane highlighted the existence of a reorientational process along the alkane chain, which is likely to be analogous to the butyl chain relaxation process within the ionic liquid. Similarly, QENS has been applied to address the dynamical behavior of the alkyl chains in dicopper tetrapalmitate.[29] Using selectively deuterated alkyl groups, increasing degrees of conformational disorder were found along the alkyl chain as the terminal methyl is approached. A similar effect has been observed from careful inspection of molecular dynamics simulation of [bmim][PF_6].[30] A recent simulation study by Ribeiro et al.[13] qualitatively showed the complex nature of the dynamics of the butyl chain attached to [bmim]Cl. Although not in the liquid state, a high degree of polymorphism has also been noted in imidazolium salts, in general those associated with halide counterions[5−7] but also in $[PF_6]^-$ materials. In many cases, the polymorphic behavior has been associated with changes in the alkyl chain orientation with respect to the imidazolium ring or within the alkyl chain. For example, [C_{14}mim]Cl·H_2O exists in two polymorphic forms where the arrangement of the cation headgroup and the alkyl chain is strongly dependent on the thermal history of the salt.[31] Similarly, crystal−crystal phase transitions have been observed in $[C_{14}mim]^+$ and $[C_{16}mim]^+$ based hexafluorophosphate ionic liquids, whereby the long alkyl chain has significantly more degrees of freedom in the high temperature structure.[32] Recently, Hamaguchi and co-workers have shown that, in short alkyl chain length ionic liquids, namely, [bmim]Cl and [bmim]Br, rotational isomers are possible where the alkyl chains contain trans−trans and trans−gauche configurations.[6,7] It is likely that the dynamical processes observed herein of the butyl chain are associated with transitions through these configurations.

The rheological and conductivity behavior in RTILs has been explored among others by Angell et al.,[33] highlighting the highly fragile behavior of ionic liquids (including [bmim][PF_6]), despite their low glass transition point. Temperature dependent viscosity data have been modeled according to a VTF parametrization:

$\eta(T) = \eta_0 \exp[B/(T - T_0)]$, with $\eta_0 = 2.0 \times 10^{-2}$ cP, $B = 1576$ K, and $T_0 = 132$ K.[34] Although the activation barrier for the rheological process is similar to the diffusive process, 13.1 kJ mol^{-1} for the viscosity compared to the value 17.1 kJ mol^{-1} that is derived in the present study, the fact that the viscosity may be fitted to an Arrhenius type of temperature dependence, whereas this is not possible for the diffusive process, shows that the dynamics probed in each case are different. However, this finding is not surprising, since in the QENS experiments the incoherent scattering measured from hydrogen atoms is related to the self-particle motion of these atoms while in a viscosity measurement the mutual interactions between different sample portions are probed. Moreover, the QENS study refers to a microscopic spatial scale, of the order of few angstroms, where self-diffusive processes are expected to have a very different nature than bulk diffusion. Currently, studies of fully deuterated samples are being undertaken in order to access information on the collective dynamics at a microscopic spatial scale which could be more directly related to rheological properties.

Conclusions

For the first time, inelastic fixed energy scans from protiated, methyl-deuterated and butyl-deuterated [bmim] [PF_6] have been examined in order to complement elastic fixed energy data as a function of temperature. Information has been extracted concerning the phase diagram of this salt, identifying the crystallization/melting point and conditions whereby the efficient characterization of the glassy amorphous phase without the occurrence of crystallization events may be achieved. This complete set of measurements allows the identification of three different dynamic processes occurring at a frequency of $\omega = 14.15$ μeV between 10 and 400 K.

The Q dependence of these processes indicates that they are related to the relaxation of the methyl and butyl groups (at low temperature) and to the diffusive dynamics above the glass transition. Upon fitting these data sets, it is found that:

(i) the methyl group relaxation occurs at very low temperature and can be described in terms of a Debye relaxation with a very low Arrhenius activation energy ($E_a = 1.28$ kJ mol^{-1}),

(ii) the butyl group relaxation can also be described in terms of a Debye relaxation with an Arrhenius-like temperature dependence ($E_{act,butyl} = 11.34$ kJ mol^{-1}),

(iii) both the methyl and butyl relaxations can be described without the introduction of a distribution of activation energies, and

(iv) the diffusive process could be described using a Kohlrausch−Williams−Watts expression ($\beta = 0.42$) and assuming a Vogel−Fulcher−Tamman temperature dependence ($E_{act,app} = 17.1$ kJ mol^{-1}; $T_0 = 170$ K). This temperature dependence differs from that which describe viscosity, as expected as the incoherent QENS technique probes only self-diffusion processes.

These data and the detailed information which may be extracted from them show the potential of the IFES technique in highlighting in a direct way the existence and nature of relaxation processes in materials.

Acknowledgment. We acknowledge the support of the European Community−Access to Research Infrastructure action of the Improving Human Potential Program (RII3-CT-2003-505925), which funded the access to the FZJ facilities. We also acknowledge funding from the ILL supporting the experiments at IN16 and IN10.

References and Notes

(1) Welton, T. *Chem. Rev.* **1999**, *99*, 2071.
(2) Margulis, C. J.; Stern, H. A.; Berne, B. J. *J. Phys. Chem. B* **2002**, *106*, 12017.
(3) Hanke, C. G.; Price, S. L.; Lynden-Bell, R. M. *Mol. Phys.* **2001**, *99*, 801.
(4) Morrow, T. I.; Maginn, E. J. *J. Phys. Chem. B* **2002**, *106*, 12807.
(5) Holbrey, J. D.; Reichert, W. M.; Nieuwenhuyzen, M.; Johnston, S.; Seddon, K. R.; Rogers, R. D. *Chem. Commun.* **2003**, 1636.
(6) Saha, S.; Hayashi, S.; Kobayashi, A.; Hamaguchi, H. *Chem. Lett.* **2003**, *32*, 740.
(7) Hayashi, S.; Ozawa, R.; Hamaguchi, H. *Chem. Lett.* **2003**, *32*, 498.
(8) Hardacre, C.; Holbrey, J. D.; McMath, S. E. J.; Bowron, D. T.; Soper, A. K. *J. Chem. Phys.* **2003**, *118*, 273.
(9) Hardacre, C.; McMath, S. E. J.; Nieuwenhuyzen, M.; Bowron, D. T.; Soper, A. K. *J. Phys.: Condens. Matter* **2003**, *15*, S159.
(10) Triolo, A.; Russina, O.; Arrighi, V.; Juranyi, F.; Janssen, S.; Gordon, C. M. *J. Chem. Phys.* **2003**, *119*, 8549.
(11) Antony, J. H.; Mertens, D.; Dolle, A.; Wasserscheid, P.; Carper, W. R. *ChemPhysChem* **2003**, *4*, 588.
(12) Giraud, G.; Gordon, C. M.; Dunkin, I. R.; Wynne, K. *J. Chem. Phys.* **2003**, *119*, 464.
(13) Urahata, S. M.; Ribeiro, M. C. C. *J. Chem. Phys.* **2004**, *120*, 1855.
(14) Hardacre, C.; Holbrey, J. D.; McMath, S. E. J. *J. Chem. Soc., Chem. Commun.* **2001**, 367.
(15) Gordon, C. M.; Holbrey, J. D.; Kennedy, A. R.; Seddon, K. R. *J. Mater. Chem.* **1998**, *8*, 2627.
(16) Russina, O.; Triolo, A.; Aihara, Y.; Telling, M. T. F.; Grimm, H. *Macromolecules* **2004**, *37*, 8653.
(17) Chahid, A.; Alegria, A.; Colmenero, J. *Macromolecules* **1994**, *27*, 3282.
(18) See, e.g.: Frick, B.; Fetters, L. J. *Macromolecules* **1994**, *27*, 974. Ahumada, O.; Theodorou, D. N.; Triolo, A.; Arrighi, V.; Karatasos, K.; Ryckaert, J.-P. *Macromolecules* **2002**, *35*, 7110.
(19) Fulcher, G. S. *J. Am. Ceram. Soc.* **1925**, *8*, 339.
(20) Vogel, H. *Phys. Z.* **1921**, *22*, 645.
(21) Tammann, G.; Hesse, W. *Z. Anorg. Allg. Chem.* **1926**, *156*, 245.
(22) Williams, G.; Watts, D. C. *Trans. Faraday Soc.* **1970**, *66*, 80.
(23) Ferguson, R.; Triolo, A.; Arrighi, V. Manuscript in preparation, 2005.
(24) Grapengeter, H. H.; Alefeld, B.; Kosfeld, R. *Colloid Polym. Sci.* **1987**, *265*, 226.
(25) Mukhopadhyay, R.; Alegria, A.; Colmenero, J.; Frick, B. *Macromolecules* **1998**, *31*, 3985.
(26) Wilson, E. B., Jr. *Adv. Chem. Phys.* **1959**, *2*, 367.
(27) Tokuda, H.; Hayamizu, K.; Ishii, K.; Susan, M.; Watanabe, M. *J. Phys. Chem. B* **2004**, *108*, 16593.
(28) Bradley, K. F.; Chen, S.-H.; Brun, T. O. *J. Chem. Phys.* **1991**, *95*, 5273.
(29) Carpentier, L.; Bee, M.; Giroud-Godquid, A. M.; Maldivi, P.; Marchon, J. C. *Mol. Phys.* **1989**, *68*, 1367.
(30) Maginn, E. J.; Morrow, T. I.; Triolo, A. Unpublished results
(31) Downard, A.; Earle, M. J.; Hardacre, C.; McMath, S. E. J.; Nieuwenhuyzen, M.; Teat, S. J. *Chem. Mater.* **2004**, *16*, 43.
(32) De Roche, J.; Gordon, C. M.; Imrie, C. T.; Ingram, M. D.; Kennedy, A. R.; Lo Celso, F.; Triolo, A. *Chem. Mater.* **2003**, *15*, 3089.
(33) Xu, W.; Cooper, E. I.; Angell, C. A. *J. Phys. Chem. B* **2003**, *107*, 6170−6178.
(34) Seddon, K. R.; Stark, A.; Torres, M. J. *ACS Symp.Ser.* **2002**, *819*, 34.